scientific reports

Check for updates

OPEN

Investigation of the temperature influence on the catalytic hydrogenation upgrading of bio-oil using industrial nickel based catalyst RZ409

Xingmin Xu[1,2]✉, Shuwan Chen[1,2], Yinju Wang[1,2], Ping Lv[1,2], Wan Guo[1,2] & Youju Shu[3]✉

Temperature and catalyst are critical factors influencing the catalytic hydrogenation of bio-oil. This study employed the industrial Ni-based catalyst RZ409 as the research subject and systematically evaluated its applicability at various reaction temperatures (200, 250, 280, 300, and 330 °C). The oil phase yield, oil properties, and chemical composition were analyzed to determine the optimal temperature. Thermogravimetric analysis (TG), X-ray diffraction (XRD), Fourier transform infrared spectroscopy (FTIR), and Brunauer-Emmett-Teller (BET) surface area analysis were utilized to evaluate the influence of temperature on the carbon deposition characteristics of the catalyst. Results showed that the optimum temperature of catalyst RZ409 is 300 °C. At this temperature, the weight factor (WF) reaches a maximum of 26.5%, balancing oil phase yield (39.7%) and oxygen removal efficiency (66.6%). The oil quality improves significantly, with water content reduced to 2.0% and calorific value increased to 37.1 MJ·kg^{-1}. TG, XRD, FTIR, and BET surface area analysis confirmed that carbon deposition on the catalyst can be effectively removed by combustion, with a low activation energy of 31.35 kJ·mol^{-1} at 300 °C. This study provides valuable theoretical and experimental support for the industrial application of bio-oil catalytic hydrogenation upgrading technology.

Keywords Bio-oil, Catalytic hydrogenation, Industrial Ni-based catalyst, Reaction temperature, Carbon deposition, Combustion kinetics

The excessive reliance on fossil energy has resulted in environmental degradation and an impending energy crisis, compelling humanity to explore alternative and sustainable energy sources[1]. Biomass stands out as the sole carbon-based renewable energy resource on Earth, characterized by its low sulfur, low nitrogen content, and zero net carbon emissions[2]. In the context of global efforts to achieve the dual-carbon goals of "carbon peak" and "carbon neutrality", biomass energy assumes particular significance[3]. Among various conversion methods, the fast pyrolysis of biomass into liquid fuel is considered one of the most promising approaches for utilizing biomass energy[4]. This dark red-brown or black liquid, referred to as biomass pyrolysis oil (bio-oil), is produced under anaerobic conditions at a reaction temperature of 450–550 °C with a short residence time (typically ≤ 2 s)[5,6]. However, bio-oil exhibits complex characteristics, including high water and oxygen content (with oxygen levels reaching up to 50%), low heating value, high viscosity and acidity, strong corrosiveness, and poor stability, rendering it unsuitable for direct use as a transportation fuel[7]. Consequently, hydrogenation upgrading is essential to enhance the quality of bio-oil[8]. As a substitute for fossil fuels, bio-oil plays a crucial role in restructuring the energy landscape, promoting energy conservation, reducing emissions, and safeguarding the environment[9].

It is widely recognized that catalysts play a pivotal role in the upgrading of bio-oil. In particular, metal-based catalysts, which include both noble and transition metals, are essential for driving key reactions such as hydrogenation, hydrodeoxygenation, and reforming[10]. Noble metal catalysts, such as rhodium, palladium,

[1]School of Basic Medicine and Forensic Medicine, Henan University of Science and Technology, No. 263, Kaiyuan Avenue, Louyang 471000, Henan, China. [2]Institute of Special Medicine, Henan University of Science and Technology, No. 263, Kaiyuan Avenue, Louyang 471000, Henan, China. [3]School of Life Science and Health Engineering, Luoyang Institute of Science and Technology, Luoyang 471003, China. ✉email: xxm78v@haust.edu.cn; jackshiwsh@163.com

platinum, and ruthenium-based catalysts, exhibit superior activity and selectivity in the catalytic upgrading of bio-oil and its model compounds[11–14]. However, the widespread application of noble metal catalysts in bio-oil upgrading is hindered by their limited availability and high cost. Transition metal catalysts, primarily Ni-based catalysts, are extensively used for the catalytic hydrogenation of bio-oil. These include Ni-based catalysts[15,16], Ni-Cu[17], Ni-Co[18,19], Ni-Mo[20], and Ni-B[21] composite catalysts. Among these, Ni-based catalysts are favored due to their excellent hydrogenation performance, relatively low cost, and ease of accessibility.

Previous studies have demonstrated significant progress in the development of Ni-based catalysts for bio-oil hydrodeoxygenation (HDO). Yang et al.[15], successfully synthesized a low-loading (1 wt%) Ni/γ-Al_2O_3 catalyst and evaluated its HDO performance using anisole as a bio-oil model compound. Under optimized conditions (WHSV = 81.6 h^{-1}), the catalyst achieved near-complete conversion (~ 100%) with 70% selectivity toward aromatic hydrocarbons, highlighting its efficiency in oxygen removal. In a comparative study, Schmitt et al.[16] investigated high-loading Ni-based catalysts for the hydrotreatment of beech wood fast pyrolysis bio-oil, benchmarking their performance against a Ru/C noble metal catalyst. While both catalysts exhibited comparable deoxygenation activity, the Ni-based system demonstrated superior hydrogenation capability and higher yields of upgraded oil-phase products. Following a two-step upgrading process, the treated bio-oil exhibited a 90% reduction in water content, a 64.8% decrease in oxygen content, and a 90.1% enhancement in heating value. However, aromatic hydrocarbon polymerization during the secondary upgrading step raised concerns regarding potential clogging in continuous reaction systems. Further advancements were reported by Wang et al.[17], who explored the synergistic effects of bimetallic Ni-Cu/HZSM-5 catalysts modified with CeO_2 for bio-oil HDO. With 15 wt% CeO_2 incorporation, the upgraded oil yield increased from 33.9 wt% (unmodified catalyst) to 47.6 wt%, while coke deposition decreased dramatically from 41 wt% to 14 wt%, indicating improved catalyst stability and resistance to deactivation. Recent literature has highlighted novel Ni-based catalysts with exceptional catalytic performance and innovative potential in biomass conversion and bio-oil upgrading[18–21]. However, these catalysts often encounter challenges associated with complex preparation procedures and minipreparation, which hinder their ability to satisfy the requirements of accessibility for industrial applications. Furthermore, their application is largely confined to small-scale laboratory studies under specific experimental conditions, leaving a significant gap before achieving industrial applicability. Consequently, identifying a Ni-based catalyst suitable for bio-oil catalytic upgrading and possessing industrial application potential not only holds substantial practical significance but also promises considerable economic benefits.

However, catalysts employed in the complex systems of bio-oil upgrading must exhibit not only exceptional hydrogenation activity but also robust resistance to carbon deposition, superior thermal stability, and appropriate acidity. The industrial Ni-based catalyst RZ409 (the reduced form of Z409), developed by China's Qilu Petrochemical, is specifically designed for naphtha catalytic reforming to produce hydrogen, demonstrating outstanding catalytic activity and thermal stability. This catalyst has been utilized in biomass gasification tar removal studies, showcasing remarkable anti-coking properties[22]. In our earlier research, the RZ409 catalyst was effectively applied for in-situ catalytic hydrogenation upgrading of bio-oil and its model compounds (phenol and furfural), revealing superior in-situ hydrogenation activity and carbon deposition resistance[23,24]. Furthermore, RZ409 is a commercially available Ni-based catalyst with proven thermal stability and anti-coking performance, offering potential cost and scalability advantages over laboratory-synthesized catalysts. Successful validation could expedite the industrial adoption of bio-oil upgrading by leveraging established catalyst supply chains. Building upon these preliminary findings, this study selects the industrial Ni-based RZ409 catalyst for bio-oil catalytic hydrogenation upgrading, aiming to confirm its applicability in bio-oil hydrogenation reactions.

In addition, temperature serves as a critical factor in the catalytic hydrogenation of bio-oil. Bio-oil exhibits significant thermal instability, and its properties profoundly influence the reaction behavior under varying temperatures[25]. Specifically, at 100 °C, bio-oil undergoes polymerization, at 200 °C, coking reactions begin to occur, when the temperature reaches 300 °C, carbon deposition forms, leading to catalyst deactivation[26]. Despite extensive literature reporting on the effects of temperature on the catalytic hydrogenation of bio-oil[27–29], there remains a lack of systematic studies analyzing the comprehensive impact of temperature on the entire process with a specific catalyst. Reaction temperature not only directly influences the quality and composition of the refined bio-oil but also significantly affects the degree of coking and the level of carbon deposition on the catalyst, further impacting the feasibility of catalyst regeneration[28]. Based on this, the objective of this study is to evaluate the applicability of the industrial Ni-based catalyst RZ409 in the catalytic hydrogenation of bio-oil and conduct an in-depth analysis of the specific effects of temperature on three aspects: first, the influence of temperature on the catalytic hydrogenation of bio-oil; second, the effect of temperature on carbon deposition of the RZ409 catalyst; third, the mechanism of temperature on the combustion kinetics of carbon deposition of the RZ409 catalyst. Through this research, it is anticipated to provide theoretical support and technical guidance for advancing the industrial development of bio-oil catalytic hydrogenation technology.

Results and discussion

The effect of temperature on bio-oil upgrading

Effect of temperature on product composition and yield

Reaction temperature is a critical factor that significantly influences the yield and composition of the products. The compositional distributions of the products at various reaction temperatures are illustrated in Fig. 1. As the temperature increases from 200 °C to 330 °C, the quantity of oily products decreases markedly from 86.7 g to 46.9 g, while the amount of gas-phase products rises from 9.1 g to 38.2 g. The yields of aqueous products remain relatively stable at approximately 37–39 g. Additionally, the quantity of solid-phase products increases from 9.5 g to 16.7 g, with material balances ranging between 87% and 93% within this temperature range. Notably, 280 °C serves as the inflection point temperature. Above this temperature, the production of oil-phase products

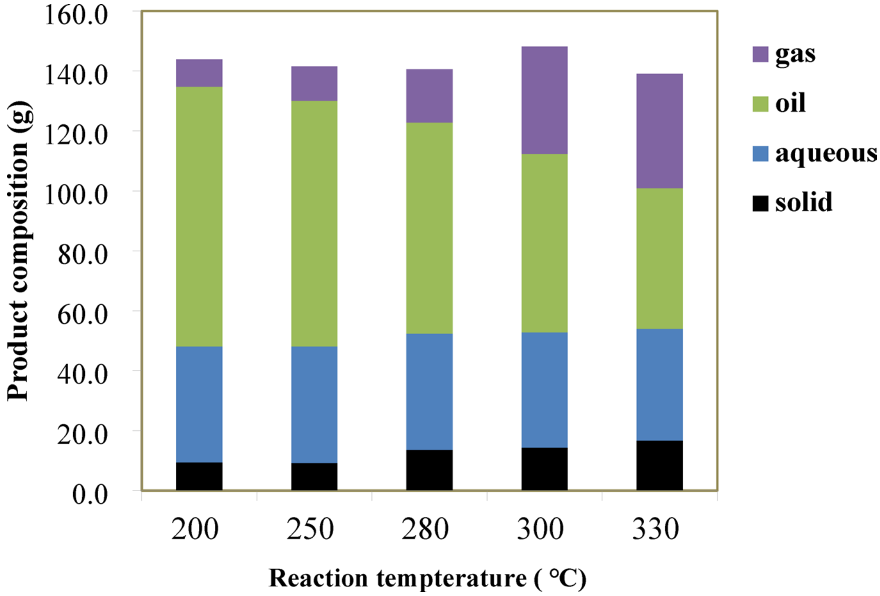

Fig. 1. The composition of the products at different reaction temperatures (initial hydrogen pressure of 2.0 MPa, reaction time of 2 h, and RZ409 catalyst dose of 10 g).

	Reaction temperature (°C)						
Elemental analysis	**Bio-oil**	**Reactant**	**200**	**250**	**280**	**300**	**330**
C (%)	36.7	49.5	66.5	67.7	67.9	76.2	76.9
H (%)	8.4	9.6	10.4	10.1	10.6	10.2	10.6
O (%)	50.2	37.7	22.3	21.2	20.5	12.6	11.5
N (%)	0.9	0.6	0.9	1.0	1.0	1.1	1.0
Properties							
Moisture (%)	34.5	23.0	6.3	5.4	4.7	2.0	1.7
HHV (MJ/kg)	14.8	22.9	32.1	33.0	33.1	37.1	38.2
DOD (%)	--	--	40.8	43.7	45.6	66.6	69.5
Y_{obs} (%)	--	--	57.8	54.7	46.9	39.7	31.3

Table 1. Elemental composition and properties of bio-oil, reactant and products at different temperature. The reactant is a mixture of 100 g bio-oil, 30 g n-butanol and 20 g xylene.

declines substantially, whereas the generation of gas-phase and solid-phase products increases. Simultaneously, polymerization and coking reactions occur, leading to increased carbon accumulation[30].

Influence of temperature on chemical properties of oil phase products

As presented in Table 1, catalytic reactions conducted at varying temperatures over the catalyst RZ409 resulted in oil-phase products with superior elemental compositions and properties compared to bio-oil and reactants. Specifically, the carbon content increased substantially from 49.5% to a range of 66.5%-76.9%, while the hydrogen content rose slightly from 9.6% to over 10%. Conversely, the oxygen content decreased significantly from 37.7% to below 22.3%, and the moisture content dropped markedly from 23% to less than 6.3%. These changes led to a substantial improvement in calorific value, which increased from 22.9 MJ kg^{-1} to between 32.1 and 38.2 MJ kg^{-1}. This phenomenon can be attributed to the transfer of moisture generated by the hydrodeoxygenation reaction to the aqueous phase, facilitating the separation of oil and water. Additionally, the removal of oxygen enhanced the carbon and hydrogen contents, thereby increasing the calorific values of the oil-phase products.

Simultaneously, based on the data analysis presented in Table 1, as the reaction temperature increased from 200 °C to 330 °C, the oxygen removal rate of oil-phase products significantly rose from 40.8 to 69.5%. Conversely, the yield of oil-phase products exhibited a downward trend, decreasing from 57.8 to 31.3%. This phenomenon can be attributed to the fact that as the reaction temperature increases, the components within the oil-phase products may undergo secondary cracking or reforming reactions, leading to an increase in gas-phase products. Additionally, high-temperature conditions promote the polymerization and coking reactions of bio-oil, thereby increasing the production of solid-phase products (as illustrated in Fig. 1).

Moreover, Fig. S1 depicts the influence curve of temperature on the yield and deoxygenation degree of oil-phase products. As shown in Fig. S1, when the reaction temperature rises from 200 °C to 280 °C, the oxygen removal rate of oil-phase products increases gradually, while its yield decreases progressively. Within the range of 280 °C to 300 °C, the oxygen removal rate accelerates sharply (by up to 21%). In the range of 300 °C to 330 °C, the oxygen removal rate again stabilizes with only a marginal increase (approximately 3%), whereas the yield of oil-phase products continues to decline rapidly (by 15.6%). Consequently, 280 °C is identified as the intersection temperature of the two curves, signifying that this temperature serves as the critical inflection point of the reaction system.

To resolve the contradiction between temperature effects on oil-phase yield and oxygen removal rate, we introduced a weight factor (WF) parameter, defined as the product of oil-phase yield and oxygen removal rate, to optimize the reaction temperature. As depicted in Fig. S2, from 200 °C to 250 °C, the curve exhibited a gentle increase, suggesting that the influence of reaction temperature was well-balanced. From 250 °C to 280 °C, the curve demonstrated a downward trend, indicating that the reduction in oil-phase yield dominated during this temperature range. From 280 °C to 300 °C, the curve showed a rapid upward trend, signifying that the oxygen removal rate became the predominant factor. From 300 °C to 330 °C, the curve displayed a sharp decline, implying that the reduction in oil-phase yield regained dominance. The WF reached its minimum value (21.4%) at 280 °C, which corresponded to the inflection point temperature, consistent with the aforementioned experimental conclusions. Conversely, the WF peaked at 300 °C (26.5%), identifying this temperature as the optimal reaction temperature, where the combined benefits of oil-phase yield and oxygen removal rate were maximized.

This conclusion is similar with the reported optimal temperature range (250–320 °C) for bio-oil catalytic hydrogenation in the existing literature, where 320 °C has been identified as the optimal reaction temperature[31]. The observed discrepancies primarily arise from two methodological factors: (1) feedstock heterogeneity. In our study, the bio-oil was derived from the fast pyrolysis of peanut shells and is a mixture of bio-oil with n-butanol and xylene, whereas in the literature baseline, the bio-oil was obtained via pyrolysis of biomass derived from biogas processes and conditioned with waste vegetable oil; (2) catalyst system divergence. In the current work, Ni-RZ409 (industrially produced, SiO_2-Al_2O_3 supported) was employed, whereas the literature reference utilized Co-Mo/γ-Al_2O_3-HMS (laboratory-synthesized).

Nevertheless, bio-oils derived from different raw material sources may exhibit significant variations in properties such as moisture content, calorific value, and composition. Despite these differences, bio-oils produced by rapid pyrolysis of biomass typically share common characteristics, including complex composition, poor thermal stability, and strong corrosiveness. Consequently, identifying suitable reaction temperature ranges holds universal significance for the application of various bio-oils. However, due to the inherent property variations among bio-oils originating from different sources, their specific optimal reaction temperatures will inevitably differ.

Component analysis of oil phase products

Table 2 presents the GC-MS analysis results of the major components in the oil-phase products obtained under 300 °C reaction conditions. As shown in table 2, apart from the added organic solvents (n-butanol, xylene: o-xylene, m-xylene, and p-xylene), a significant amount of ester compounds were detected in the product, accounting for approximately 5.3%. These esters, including acetic acid Butyl ester, Butanoic acid Butyl ester, pentanoic acid Butyl ester, and hexanoic acid Butyl ester, were formed through the reaction between acids in bio-oil and the n-butanol solvent, as previously reported in our earlier study[32].

Additionally, a substantial proportion of alkanes (approximately 41.6%) were identified in the product. However, some of these alkanes likely originated from the isomerization reactions of the added xylene, such as ethylbenzene, 1-methylethyl-benzene, and 1-ethyl-3-methyl-benzene. Furthermore, small amounts of unreacted acids (e.g., acetic acid, propanoic acid, Butanoic acid, pentanoic acid, and hexanoic acid) were observed in the oil-phase product, comprising approximately 1.6% of the total composition. Phenolic compounds, including phenol, 2-methoxy-phenol, and 2,6-dimethoxy-phenol, accounted for approximately 2.6% of the total product. This can be attributed to the relative stability of phenolic compounds, which are less prone to HDO reactions. Under more rigorous experimental conditions, phenolics can potentially be converted into hydrocarbon compounds, such as aromatic hydrocarbons or cycloalkanes[33].

The effect of temperature on coke deposition

Thermogravimetric analysis (TGA)

Figure 2 shows the thermogravimetric curves of the RZ409 catalyst at different reaction temperatures. This figure shows that before a combustion temperature of 200 °C, the catalyst at each reaction temperature exhibited only a small weight loss (< 3%), which was caused by the volatilization of a small amount of organic matter attached to the catalyst. When the combustion temperature was 250 °C, the catalysts began to lose weight obviously (except at 330 °C). The combustion temperature range from 250 °C to 450 °C showed a rapid weight loss stage for each catalyst due to carbon deposition on the catalyst undergoing combustion and conversion to CO_2. Above a combustion temperature of 450 °C, the weight losses of each catalyst tended to stabilize (except for 330 °C a, b). The weight losses of the catalyst used at 200 °C, 250 °C and 280 °C were 20.2%, 22.4% and 28.9% (Table 3), respectively, which showed that the higher the reaction temperature was, the greater the extent of carbon deposition on the catalyst. However, when the reaction temperature was 300 °C, the total weight loss of the catalyst was 23.1% (Table 3), which was 5.8% less than that at 280 °C, indicating that the carbon deposition degree of the catalyst was weakened. This is because under the experimental conditions of 300 °C and 11 MPa, the added n-butanol solvent is in its supercritical state (supercritical condition of n-butanol: 287 °C, 4.9 MPa). At this point, supercritical n-butanol has a stronger diffusion and dissolution ability that effectively reduces the mass transfer and heat transfer resistance of the reaction system and effectively inhibits the coking reaction of bio-oil polymerization, thereby decreasing the extent of carbon deposition on the catalyst[32].

No.	Retention time (min)	Chemical compositions	Area (%)
1	4.16	**Acetic acid, butyl ester**	**4.13**
2	5.27	**Ethylbenzene**	**40.29**
3	5.44	**o-Xylene**	7.04
4	5.60	**Benzene, 1,3-dimethyl-**	18.17
5	5.69	**1-Butanol**	14.30
6	6.33	Benzene, (1-methylethyl)-	0.30
7	6.68	**p-Xylene**	7.42
8	6.93	Cyclopentanone, 2-methyl-	0.46
9	7.28	Benzene, propyl-	0.50
10	7.60	**Butanoic acid, butyl ester**	**0.63**
11	7.76	Benzene, 1-ethyl-3-methyl-	0.50
12	9.64	Cyclopentanone, 2-ethyl-	0.22
13	10.54	**Pentanoic acid, butyl ester**	0.26
14	13.67	**Hexanoic acid, butyl ester**	0.25
15	15.08	Acetic acid	0.36
16	15.79	Cyclohexanone, 2-butyl-	0.39
17	15.88	1 H-Inden-1-one, octahydro-7a-hydroxy-	0.21
18	16.13	Cyclopentanone, 2-(1-methylpropyl)-	0.55
19	17.76	Propanoic acid	0.25
20	20.45	Butanoic acid	0.46
21	23.66	Pentanoic acid	0.24
22	25.11	2-Hexanoylfuran	0.21
23	26.66	Hexanoic acid	0.34
24	27.24	Phenol, 2-methoxy-	0.44
25	29.78	Phenol, 2-methoxy-4-methyl-	0.30
26	31.06	Phenol	0.39
27	32.99	Phenol, 3,4-dimethyl-	0.38
28	33.57	Phenol, 2-methoxy-4-propyl-	0.44
29	37.54	Phenol, 2,6-dimethoxy-	0.27
30	38.09	Phenol, 2-(1-methylpropyl)-, methylcarbamate	0.33

Table 2. Major compounds of upgraded bio-oil determined by GC-MS (A original table report of upgraded bio-oil components from GC-MS is shown in Table S2).

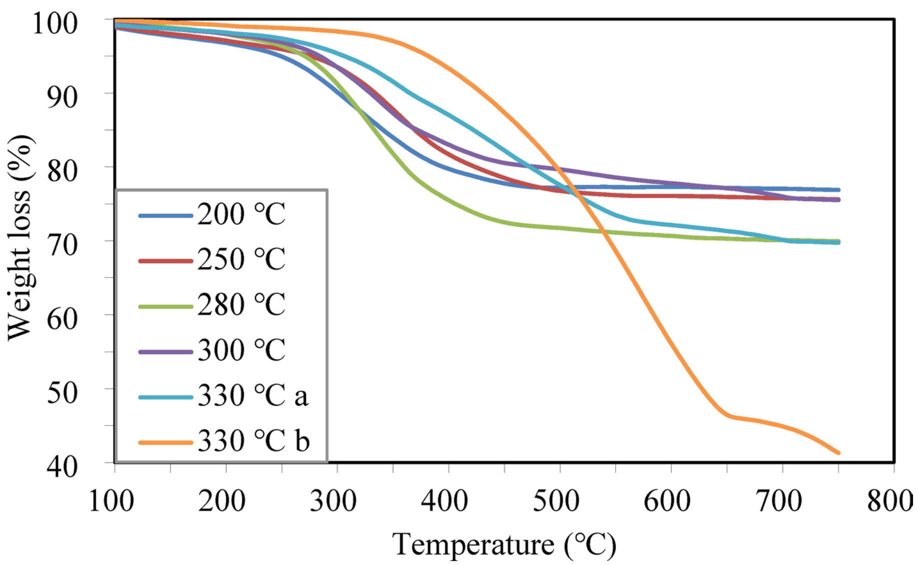

Fig. 2. Thermogravimetric analysis of the RZ409 catalysts used at different temperatures.

Reaction temperatures (°C)	200	250	280	300	330 a	330 b
Weight losses (%)	20.2	22.4	28.9	23.1	29.3	58.1

Table 3. Weight loss values of the used catalyst RZ409 determined by TG analysis.

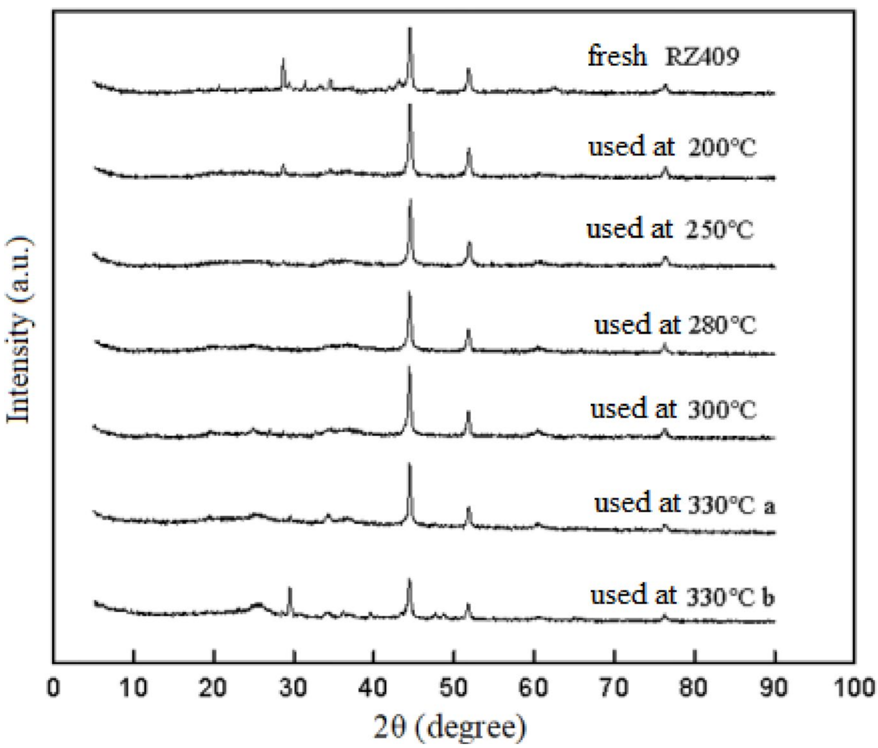

Fig. 3. XRD pattern of the fresh RZ409 and used catalyst at different temperatures (330 °C a-recovery catalyst in the liquid phase; 330 °C b-recovery catalyst in the solid phase).

However, when the reaction temperature was further elevated to 330 °C, the supercritical conditions of n-butanol were insufficient to suppress the coking reaction, leading to the formation of a significant amount of carbon deposits. The catalyst (330 °C a), which was separated from the oil phase, experienced a weight loss of 29.3%, and its weight loss curve stabilized at 550 °C. Meanwhile, the solid-phase product (330 °C b) in the reactor exhibited a weight loss of 58.1%, with a combustion temperature of 650 °C. These results indicate that the type of carbon deposit formed by the solid-phase product in the reactor is markedly different from that formed by the catalyst separated from the oil phase.

X-ray diffraction analysis (XRD)

Figure 3 presents the X-ray diffraction (XRD) analysis of the RZ409 catalyst under various reaction temperatures. By comparing with the standard XRD pattern, the peaks located at 2θ = 44.5°, 51.8°, and 61.5° are assigned to the Ni crystal phase. This figure demonstrates that the Ni crystallite size of the RZ409 catalyst remains relatively unchanged within the reaction temperature range of 200 °C to 330 °C, suggesting that the active components of the RZ409 catalyst exhibit high stability in this temperature interval. The peak at 2θ = 43.9° corresponds to incompletely reduced NiO, while the peak at 2θ = 25.8° is attributed to amorphous carbon deposits observed at 330 °C (denoted as 330 °C a and 330 °C b). Furthermore, the peak at 2θ = 29.5° is associated with graphite carbon crystals, as referenced by code 00-001-0646. It is evident that the carbon deposit formed at 330 °C is graphite carbon, which aligns with the thermogravimetric (TG) analysis results. Additionally, other prominent peaks may originate from carriers or additives present in the catalyst.

Fourier transform infrared spectra (FTIR)

The infrared spectra of bio-oil and upgraded bio-oil at the optimal reaction temperature are presented in Fig. 4. As can be observed from the figure, the infrared spectral characteristics of bio-oil and upgraded bio-oil exhibit similarities. Specifically, the strong absorption peak at 3400 cm^{-1} corresponds to the stretching vibration of hydroxyl groups (-OH), the prominent absorption peak at 2900 cm^{-1} is primarily attributed to the tensile vibrations of C-H bonds in aliphatic and aromatic hydrocarbons[35]. The strong absorption peak near 1700 cm^{-1} is associated with the carbonyl group (C = O), which originates from carboxylic acids and ketones present in both bio-oil and refined bio-oil[33]. However, it has been reported that the absorption peak in this band may also

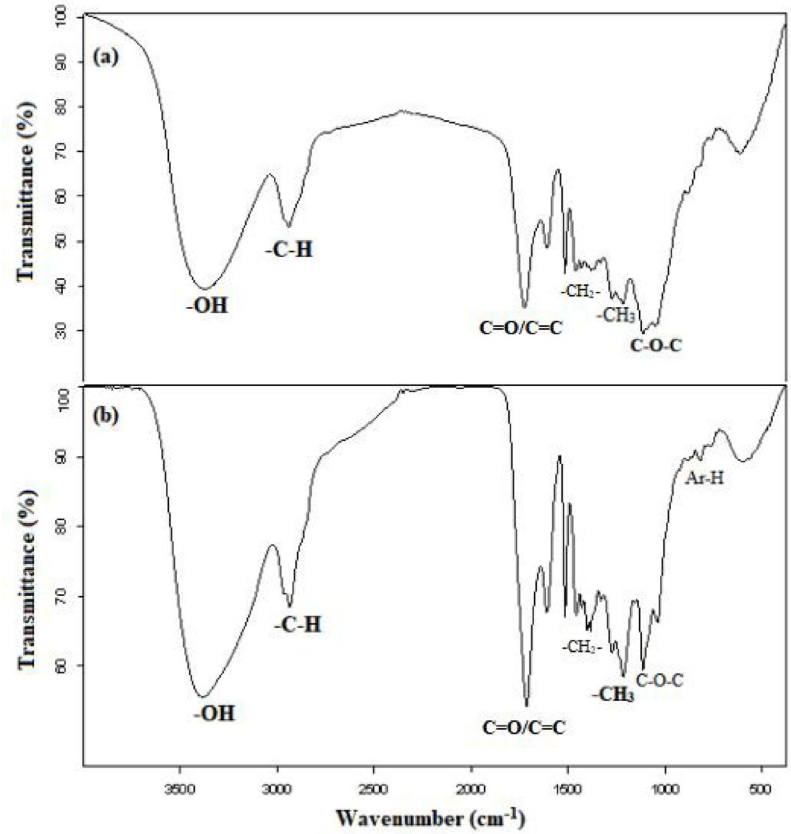

Fig. 4. FT-IR diagram (**a**) bio-oil (**b**) upgraded bio-oil (at 300°C).

correspond to the C = O vibration in ester compounds[36,37], as these studies focused on the preparation of biodiesel via esterification and transesterification reactions, where esters are the primary components. In this study, the upgraded bio-oil contains esters generated through the esterification reaction between the added butanol solvent and acidic components in the bio-oil (see Table 2). Furthermore, the absorption peak at 1600 cm^{-1} is attributed to the stretching vibration of the C = C bond in aromatic rings[35], as both bio-oil and upgraded bio-oil contain aromatic cyclic compounds (e.g., phenolic compounds), moreover the upgraded bio-oil contains a significant concentration of aromatic hydrocarbons, as detailed in Table 2. The bending vibrations of aliphatic -CH_2 and -CH_3 groups are confirmed by absorption bands in the range of 1550–1390 cm^{-1}[36]. Notably, the absorption peak near 1200 cm^{-1} indicates the presence of alkyl and alkanes functional groups (-CH_3), the absorption peak in the range of 1000–1100 cm^{-1} corresponds to the C-O-C functional group, signifying the presence of phenolic compounds[38]. According to the data in Table 2, the upgraded bio-oil still contains a substantial amount of methoxyphenol compounds.

Significant differences are evident in the FT-IR spectra of bio-oil and refined bio-oil. Specifically, the Ar-H vibration peak of aromatic hydrocarbons at 850 cm^{-1} is more pronounced in the infrared spectrum of the refined bio-oil (b) compared to that of the bio-oil (a). Additionally, the vibrational peaks of -CH_2 and -CH_3 groups are more prominent in the range of 1200–1500 cm^{-1}, indicating an improvement in bio-oil quality after catalytic treatment, consistent with previous experimental findings. In the range of 1600–1700 cm^{-1}, the peak shape of the infrared spectrum of the refined bio-oil is more distinct than that of the raw bio-oil. This is because, although the content of acids, aldehydes, and ketones decreases during the refining process, a large number of ester compounds are formed, preserving the vibrational characteristics of C = O. Simultaneously, the addition of xylene solvent in the reaction system increases the aromatic hydrocarbon content, enhancing the C = C vibration peak of the aromatic ring. In addition, despite the upgraded bio-oil thought catalytic refining treatment, the -OH peak at 3400 cm^{-1} remains strong due to the continued presence of phenolic hydroxyl and alcohol hydroxyl functional groups in the product.

The used catalysts employed at 300 °C and 330 °C were characterized using FTIR, as depicted in Fig. 5. The FTIR spectra revealed that the O-H bond stretching vibration peak was located at 3400 cm^{-1}, the aliphatic C-H stretching vibration peak was observed at 2900 cm^{-1}, the C = O/C = C stretching vibration peak appeared within the range of 1600–1700 cm^{-1}, the C-H bending vibration peak was identified at 1400 cm^{-1}, and the Si-O-Si vibration peak was detected at 990 cm^{-1}. By comparing the two reaction temperatures, it is evident that the types of carbon deposits formed on the catalyst at 330 °C underwent significant changes: the content of alcohol hydroxyl substances decreased, while the content of aliphatic substances increased; the substances containing C = O/C = C disappeared, the content of substances with C-H bonds significantly increased, and the

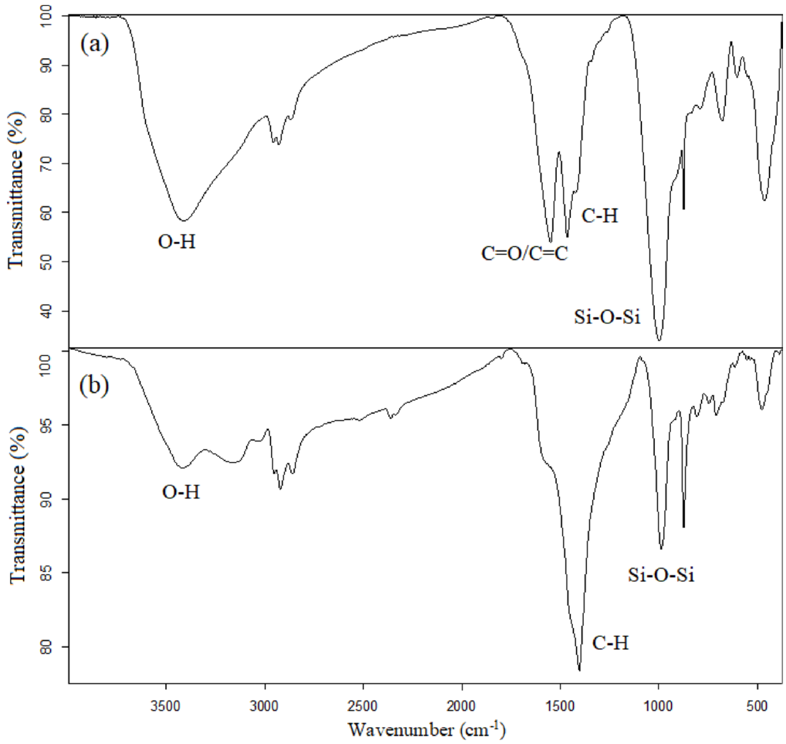

Fig. 5. FTIR spectra of the RZ409 catalyst at different reaction temperatures: (**a**) 300 °C and (**b**) 330 °C.

proportion of hydrogen decreased due to the continuous dehydrogenation of macromolecular products formed by polymerization coking.

Based on our previous studies on carbon deposition[39,40], carbon deposits can be broadly categorized into two types: soft (soluble) carbon deposits and hard (insoluble) carbon deposits. Specifically, soft carbon is highly active, soluble in organic solvents, and readily oxidized and removed, predominantly forming at reaction temperatures ranging from 200 °C to 280 °C. In contrast, hard carbon deposits exhibit a graphite-like structure with low activity and are the primary species responsible for catalyst deactivation. These deposits primarily form within the temperature range of 280 °C to 330 °C and require high-temperature treatment for removal. Consequently, the FTIR analysis suggests that carbon deposits formed at lower reaction temperatures (< 300 °C) consist predominantly of soft carbon with a higher hydrogen content, which increases with rising reaction temperature. However, graphite-like carbon deposits with lower hydrogen content began to form at 330 °C and could be eliminated through combustion at high temperatures (500–700 °C), consistent with the findings of the preceding thermogravimetric analysis.

However, the relevant literature indicates that during the process of biomass energy conversion and utilization, carbon deposits formed on the catalyst surface can be categorized into three distinct types[38]. The first type consists of non-polymerized light compounds, which can be effectively removed by washing the catalyst with organic solvents such as acetone or ethanol. The second type comprises coke with weak bonds, which can be eliminated from the catalyst surface by heating it in an oxygen-free environment. This type of coke is typically derived from the conversion of cellulose and hemicellulose compounds. The third type of coke originates from large aromatic compounds generated by lignin oligomers and is presumed to be removable through combustion (although the specific removal method for this type of coke unclear in the literature). In fact, the first and second types of carbon deposits described in the literature align closely with what we define as soft carbon deposits, whereas the third type corresponds to hard carbon deposits. This classification discrepancy arises primarily due to variations in reaction scenarios and the types of catalysts employed, leading to differences in the forms of carbon deposition, which are further differentiated based on their respective removal methods.

BET surface area analysis

Table 4 presents the experimental data of the specific surface area of fresh RZ409 catalyst and RZ409 catalysts used at different reaction temperatures. It can be seen from Table 4 that the specific surface area of fresh RZ409 catalyst is 17.4 $m^2 g^{-1}$. Compared with the fresh catalyst, the specific surface area of RZ409 catalysts used at different reaction temperatures all decreased, and showed a trend of gradually decreasing with the increase of reaction temperature. However, at a reaction temperature of 300°C, the specific surface area of the catalyst showed an exception (slightly increased compared to the specific surface area at low temperatures), which may be attributed to the fact that the n-butanol solvent was in a supercritical state at this temperature, providing a certain protective effect on the catalyst[32]. This result is consistent with the experimental conclusion in the previous section. When the reaction temperature was further increased to 330°C, the specific surface area of

RZ409 catalyst	Fresh	Useded at different temperature (°C)					
		200	250	280	300	330a	330b
BET surface area ($m^2 g^{-1}$)	17.4	15.6	12.3	11.5	13.6	7.8	3.7

Table 4. BET of fresh and used RZ409 catalysts at different reaction temperatures.

the used catalyst decreased to 7.8 $m^2 g^{-1}$, while the specific surface area of the catalyst recovered from the solid product further decreased to 3.7 $m^2 g^{-1}$. The above results indicate that at this reaction temperature, significant carbon deposition occurred on the catalyst surface, leading to a significant decrease in its specific surface area. This conclusion is consistent with the results of TG and XRD.

Coke combustion kinetics analysis

According to the results of catalyst thermogravimetric analysis, the catalyst thermogravimetric process involves combustion of the carbon deposit on the catalyst.

The combustion reaction of carbon deposits can be expressed as f(w) = wn:

$$-\frac{dw}{dt} = kf\left(w\right) \tag{1}$$

The rate constant k can be expressed by the Arrhenius formula:

$$k = Aexp\left(-\frac{E}{RT}\right) \tag{2}$$

From formulas (1) and (2) and the heating rate β = DT/dt (K/s), the kinetic equation for.
carbon deposit combustion can be obtained:

$$-\frac{dw}{dT} = \frac{A}{\beta}exp\left(-\frac{E}{RT}\right)w^n \tag{3}$$

where w is the mass percent of unburned carbon, t is time, T is the reaction, temperature (K), R is the gas constant, 8.314 J mol^{-1} K^{-1}, A is the frequency factor (s^{-1}), E is the activation energy (J mol^{-1}), and n is the reaction order.

By using Coats and Redfern's method[41], formula (3) can be transformed into:

$$ln\left(\frac{-lnw}{T^2}\right) = ln\left[\frac{AR}{\beta\, E}\left(1-\frac{2RT}{E}\right)\right] - \frac{E}{RT}?n = 1 \tag{4}$$

$$ln\left[\frac{1-\left(w^{1-n}\right)}{T^2(1-n)}\right] = ln\left[\frac{AR}{\beta\, E}\left(1-\frac{2RT}{E}\right)\right] - \frac{E}{RT}?n \neq 1 \tag{5}$$

In general, the value of 2RT/E is much less than 1, so ln [AR/β E (1-2RT/E)] can be regarded as a constant. Therefore, when $n = 1$, the correlation between - ln [- ln w/T^2] and 1/T is used to obtain the kinetic curve of carbon deposit combustion. When $n \neq 1$, a straight line can be obtained by correlating - ln [(1-w^{1-n})/T^2 (1-n)] with 1/T (Fig. 6). According to Fig. 6, the linear slope a and intercept b of the carbon deposit combustion kinetics at each reaction temperature can be obtained, and then, the activation energy E and frequency factor A can be obtained through the linear slope a and intercept b[41,42].

The results of evaluating the combustion activation energy values of carbon deposits on the catalyst at different reaction temperatures are presented in Table 5. As shown in Table 5, the activation energy for the combustion of coke deposits on the deactivated catalyst is lowest at 200 °C, with E_1 = 20.32 kJ mol^{-1}. With increasing reaction temperature, the activation energy for the combustion of coke deposits on the deactivated catalyst also increases. At a reaction temperature of 280 °C, the activation energy reaches E_3 = 35.51 kJ mol^{-1}. However, when the reaction temperature rises to 300 °C, the activation energy decreases slightly to E_4 = 31.35 kJ mol^{-1}. Subsequently, at 330 °C, the activation energy increases again to E_5 = 36.72 kJ mol^{-1}. These results indicate that the quantity of carbon deposits on the catalyst at 300 °C is lower than that at 280 °C and 330 °C. Furthermore, the carbon deposits formed at 300 °C are easier to burn and desorb compared to those formed at 280 °C and 330 °C, which facilitates more effective catalyst regeneration.

The higher the activation energy of carbon deposit combustion, the more challenging it becomes to burn and desorb the carbon deposits from the catalyst, thereby exacerbating catalyst deactivation[42]. Catalyst regeneration is typically achieved through high-temperature oxidation to induce the combustion and desorption of carbon deposits. Higher activation energy necessitates a higher desorption temperature. However, at elevated temperatures, dealumination and severe dehydroxylation may occur within the catalyst framework. The removal of aluminum from the catalyst's framework structure creates vacancies and lattice defects, which can increase the density of L-acid centers. Nevertheless, the dehydroxylation reaction is irreversible. Dehydroxylation at B-acid

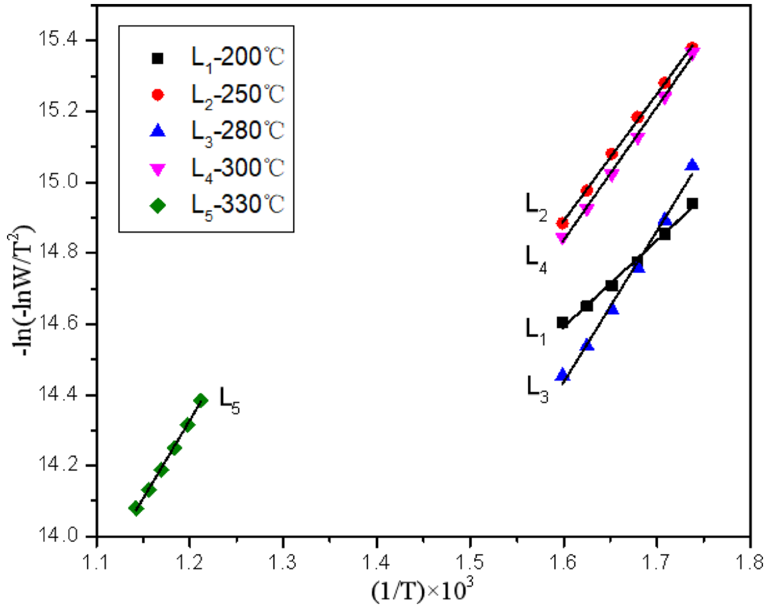

Fig. 6. Combustion kinetic curves of carbon deposits on the catalyst.

	Temperature range/K	Slope a	Intercept b	E (kJ/mol)	R_0
L_1	575–625	2.4443	10.68048	20.32	0.9962
L_2	575–625	3.5900	9.1465	29.85	0.9960
L_3	575–625	4.2709	7.6023	35.51	0.9967
L_4	575–625	3.7707	8.8029	31.35	0.9988
L_5	825 ~ 875	4.4164	9.0294	36.72	0.9995

Table 5. Calculated combustion activation energies of carbon on the catalysts. L_1: 200 °C; L_2: 250 °C; L_3: 280 °C; L_4: 300 °C; L_5: 330 °C; E: activation energy; and R_0: correlation coefficient.

sites directly results in a substantial reduction in the content of B-acid centers and the total acid quantity, thereby weakening the catalyst's acidity and significantly impacting its catalytic activity post-regeneration.

Mechanisms of temperature on the catalytic pathways

In this study, the potential influence mechanisms of temperature on catalytic pathways can be primarily categorized into two aspects. First, temperature variations significantly impact the catalytic activity of Ni-based catalysts. Specifically, an increase in temperature enhances the hydrogenation catalytic activity of Ni monomers and may alter the structural characteristics of Ni grains, thereby influencing the catalytic reaction pathways[43]. However, excessively high temperatures may lead to the aggregation or sintering of Ni grains, resulting in a decline in catalyst activity or complete deactivation[44]. Second, temperature also plays a critical role in shaping the chemical reaction pathways of bio-oil components[45]. Given the complexity and poor thermal stability of bio-oil components, a range of complex chemical reactions may occur as the temperature rises, including but not limited to hydrogenation, hydrodeoxygenation, and polymerization/coking reactions[32]. These reactions coexist and compete within a specific temperature range, with their progression closely tied to the catalytic performance of the catalyst. Notably, when the reaction temperature exceeds 330 °C, polymerization and coking reactions dominate, causing severe carbon deposition on the catalyst surface and ultimately leading to catalyst deactivation. Consequently, selecting an appropriate reaction temperature is of paramount importance in the catalytic hydrogenation process of bio-oil. Nevertheless, due to the intricate nature of the reaction system, the precise influence mechanism of temperature on catalytic pathways requires further in-depth investigation.

Conclusions

As the reaction temperature increases, the oil-phase yield decreases, while the solid-phase and gas-phase yields increase. At 280 °C, the reaction inflection point occurs. Above this temperature, the oil-phase yield drops significantly, oxygen removal accelerates, and oil quality improves markedly, indicating hydrodeoxygenation of bio-oil begins at 280 °C. At 300 °C, oxygen removal reaches equilibrium. Beyond this point, further increases in temperature reduce oil-phase yield with limited improvement in oil quality. The optimal reaction temperature range for the RZ409 catalyst is 280–300 °C, with 300 °C being most favorable.

Carbon deposition analysis shows that below 280 °C, carbon deposits increase with rising temperature. Between 280 °C and 300 °C, supercritical n-butanol reduces carbon deposits. Above 300 °C, carbon deposits rise sharply. Combustion kinetics reveal minimal activation energy for carbon deposition at 300 °C, enabling easy removal and catalyst regeneration. However, above 300 °C, carbon deposits transform into hard graphite-like residues requiring high temperatures (> 650 °C) for removal, risking catalyst support damage and complicating regeneration.

Materials and methods

Materials

Bio-oil was supplied by the fast pyrolysis of peanut shells at 500 °C in a bench-scale fluidized-bed reactor at Zhengzhou University. The industrial Ni-based catalyst RZ409 was obtained from Shandong Qilu Petrochemical Research Institute. Its main active ingredient is Ni (content 16–19%), and mixed with CaO, K_2O, LnOx additives, the carrier is SiO_2-Al_2O_3 with a certain acidity. The RZ409 solid catalyst was crushed and screened through a 200-mesh screen and set aside. The measured surface area is 17.4 m^2• g^{-1} (the properties of the catalyst are shown in Table S1). Xylene (purity 99%) and 1-butanol (purity 99.5%) were obtained from Sinopharm Chemical Reagent (Tianjin China). All reagents used were of analytical pure grade and used without further purification.

Methods

The experiments were performed in a 500 mL batch reactor equipped with a magnetic overhead stirrer, a pressure indicator and a thermocouple (Beijing Torch Petrochemical). A schematic representation of the system setup was published in an earlier paper[24]. The batch reactor was charged with the reactants (100 g bio-oil, 30 g n-butanol, and 20 g xylene) and catalyst (10 g RZ409). Subsequently, the reactor was flushed with N_2 gas, purged three times with H_2 (replacing nitrogen) and eventually pressurized with 2.0 MPa H_2 at room temperature. The reactor was heated to the intended reaction temperatures (200, 250, 280, 300 and 330 °C) with a heating rate of 3.0 °C min^{-1} and kept at that temperature for 2 h at a stirring speed of 650 rpm. The selected xylene can disperse and dilute bio-oil components, and the selected n-butanol can promote the compatibility of bio-oil and xylene. Moreover, n-butanol can be involved in the reaction, neutralizing the acids in the bio-oil. The elemental composition and properties of the bio-oil and reactants are shown in Table 1. After the reaction, the reactor was cooled to ambient temperature, the catalyst was separated from the liquid phase by filtration, and the liquid phase was then separated via a separatory funnel into the oil and water phases. Then, the oil phase and catalyst were tested and characterized.

Product analysis

The elemental compositions of both the bio-oil and oil-phase products were determined using a Thermo Electron Corporation Flash EA 1112 analyzer (Delft, the Netherlands). The higher heating values (HHVs) of the samples were measured by a ZDHW-6000 automatic calorimeter (Hebi Instrument, Henan). The water content in the samples was determined by a Karl Fischer KF-1 A automatic titration apparatus (Shanghai Baoshan Fine Working Electronic Instrument).

GC-MS analyses were performed on an Agilent 7890 A-5975 C GC system equipped with a 30 m × 0.25 mm and 0.25 mm capillary column to analyze the liquid products. The GC split was 1:100, the injector temperature was set at 250 °C, and an injection volume of 1 µL was used. The temperature program of the oven was as follows: 50 °C for 3 min, heating at 4 °C min^{-1} to 200 °C and held for 50 min at 200 °C. Helium was used as the carrier gas, with a constant flow rate of 1 mL min^{-1}. The mass spectrometry analyzer employed an electron impact ionization source energy of 70 eV. Compound spectra were obtained from the NIST08 spectra library for comparison, and the peak area normalization method was used to analyze the data.

Catalyst characterization

Thermogravimetric (TG) analyses of fresh and spent catalysts were performed on an STA-449 C TG analyzer (NETZSCH, Germany). Catalyst samples (~ 0.01 g) were placed in corundum crucibles and subsequently heated at a constant heating rate of 10 °C min^{-1} from ambient temperature to 1000 °C. All measurements were conducted in air (0.1 MPa). The weight of the carbon residue deposited on the catalyst was determined from the difference in the weight losses (after TG) of the fresh and spent catalysts.

X-ray diffraction (XRD) analyses were performed on an X'Pert PRO (PANalytical, the Netherlands) X-ray diffractometer equipped with a Cu Kα radiation source. Diffraction patterns were recorded by scanning at angles from 10 to 90° in 0.05° step increments with an acquisition period of 10 s per step.

Fourier transform infrared (FTIR) spectra of the oil phase and catalysts were recorded using a Bruker Alpha Class 1 instrument. The spent catalyst samples (1.0-1.2 mg) were pelletized with KBr (100 mg, purity > 99%), and pressures equivalent to 10 ton cm^{-2} were applied for 10 min. The operation strictly followed typical quality analysis procedures to ensure the accuracy of the results.

The total specific surface area of the catalysts were adsorbed by N_2 adsorptionn-desorption isotherms: Canta Nova 1000e (Quantachrome), and the specific surface area of the catalyst was calculated according to the Brunauer-Emmett-Teller (BET) equation for relative pressures (P/P_0) between 0.0 and 0.2[32].

Performance evaluation

The main evaluation parameters in this section are the oil-phase yield (Y_{obs}) and the degree of deoxygenation (DOD) as follows[33]:

$$Y_{obs} = \frac{m_{product}}{m_{feed}} \times 100\% \tag{6}$$

$$DOD = 1 - \left(\frac{wt\%\ O_{product}}{wt\%\ O_{feed}}\right) \times 100\% \tag{7}$$

where $m_{product}$ and m_{feed} are the masses of the product and feedstock, respectively, and wt%. $O_{product}$ and wt% O_{feed} are the percentages of oxygen in the product and feedstock, respectively.

To further investigate the effect of the reaction temperature on the catalytic hydrogenation results of bio-oil, the Y_{obs} is multiplied by the DOD, and it is defined as the weight factor (WF) as follows:

$$WF = (Y_{obs} \times \ DOD)\, 100\% \tag{8}$$

where WF is given as a percentage, this parameter indicates some equilibrium between the Y_{obs} and the DOD.

Data availability

The authors declare that the data supporting the findings of this study are available within the paper and its supplementary information files.

Received: 19 February 2025; Accepted: 29 July 2025
Published online: 04 August 2025

References

1. Ibrahim, A., Elsayed, I. & Hassan, E. B. Catalytic upgrading of rice straw bio-oil via esterification in supercritical ethanol over bimetallic catalyst supported on rice straw Biochar. *Energies* **17** (2), 407. https://doi.org/10.3390/en17020407 (2024).
2. Qiu, B. B. et al. Research progress in the Preparation of high-quality liquid fuels and chemicals by catalytic pyrolysis of biomass: A review. *Energ. Convers. Manage.* **261**, 115647. https://doi.org/10.1016/j.enconman.2022.1156 (2022).
3. Yang, M. L. et al. X. Co-pyrolysis of heavy bio-oil and disposable masks pyrolysate with Ce/Fe-based oxygen carrier catalyst. *Fuel* **336**, 127147. https://doi.org/10.1016/j.fuel.2022.127147 (2023).
4. Trinh, Q. T., Banerjee, A., Ansari, K. B., Dao, D. Q. & Le, M. T. *Upgrading of Bio-oil from Biomass Pyrolysis:Current Status and Future Development, Biorefinery of Alternative Resources: Targeting Green Fuels and Platform Chemicals* 317–353. https://doi.org/10.1007/978-981-15-1804-1_14 (2020).
5. Inayat, A. et al. Techno-economical evaluation of bio-oil production via biomass fast pyrolysis process: a review. *Front. Energy Res.* **9**, 770355. https://doi.org/10.3389/fenrg.2021.770355 (2022).
6. Kumar, R. & Strezov, V. Thermochemical production of bio-oil: A review of downstream processing technologies for bio-oil upgrading, production of hydrogen and high value-added products. *Renew. Sust Energ. Rev.* **135**, 110152. https://doi.org/10.1016/j.rser.2020.110152 (2021).
7. Hu, X. & Gholizadeh, M. Progress of the applications of bio-oil. *Renew. Sust Energ. Rev.* **134**, 110124. https://doi.org/10.1016/j.rser.2020.110124 (2020).
8. Zhang, M. Y. et al. A review of bio-oil upgrading by catalytic hydrotreatment: advances, challenges, and prospects. *Mol. Catal.* **504**, 111438. https://doi.org/10.1016/j.mcat.2021.111438 (2021).
9. da Costa, A. A. F. et al. Recent advances on catalytic deoxygenation of residues for bio-oil production: An overview. *Mol. Catal.* **518**, 112052. https://doi.org/10.1016/j.mcat.2021.112052 (2022).
10. Muhammad, S. A., Muhammad, T. N., Sajid, A. & Wajid, Z. Metal-based catalysts in biomass transformation: from plant feedstocks to renewable fuels and chemicals. *Catalysts* **15** (1), 40. https://doi.org/10.3390/catal15010040 (2025).
11. He, Y. F., Liu, R. H., Yellezuome, D., Peng, W. X. & Tabatabaei, M. Upgrading of biomass-derived bio-oil via catalytic hydrogenation with Rh and Pd catalysts. *Renew. Energ.* **184**, 487–497. https://doi.org/10.1016/j.renene.2021.11.114 (2022).
12. Nejadmoghadam, E. et al. Stabilization of fresh and aged simulated pyrolysis oil through mild hydrotreatment using noble metal catalysts. *Energ. Convers. Manage.* **313**, 118570 (2024).
13. Page, J. R. et al. Effect of Pt and Ru-based catalysts on the electrochemical hydrodeoxygenation of phenol to cyclohexane. *Catal. Sci. Technol.* **14** (19), 5559. https://doi.org/10.1039/d4cy00634h (2024).
14. Kurniawan, R. G. et al. Kim. J. Tuning surface-active sites of Ru catalysts for the selective deoxygenation of lignin monomers to fuels and chemicals. *Sci. China Chem.* **68**. https://doi.org/10.1007/s11426-024-2488-x (2025).
15. Yang, Y. X., Qiao, L. Q., Hao, J. S., Shi, H. & Lv, G. Q. Hydrodeoxygenation upgrading of bio-oil on Ni-based catalysts with low Ni loading. *Chem. Eng. Sci.* **208**, 115–154. https://doi.org/10.1016/j.ces.2019.08.012 (2019).
16. Schmitt, C. C. et al. Evaluation of high-loaded Ni-based catalysts for upgrading fast pyrolysis bio-oil. *Catalysts* **9** (9), 784. https://doi.org/10.3390/catal9090784 (2019).
17. Wang, W. H., Zhang, C. S., Chen, G. H. & Zhang, R. Q. Influence of ceo. *Addition Ni-Cu/HZSM-5 Catalysts Hydrodeoxygenation bio-oil Appl. Sci.* **9** (6), 1257. https://doi.org/10.3390/app9061257 (2019).
18. Tian, Z. P. et al. Hydrodeoxygenation of Guaiacol as a model compound of pyrolysis lignin-oil over NiCo bimetallic catalyst: reactivity and kinetic study. *Fuel* **308**, 122034 (2022).
19. Lv, Y. C. et al. Selective production of cycloalkanes through the catalytic hydrodeoxygenation of lignin with CoNi. *Int. J. Biol. Macromol.* **303**, 140496. https://doi.org/10.1016/j.ijbiomac.2025.140496 (2025).
20. Tran, Q. K. et al. One-pot depolymerization of forest residues to potential aviation fuel over hybrid zeolite N-doped activated carbon supported NiMo catalyst. *Renew. Energ.* **246**, 122835 (2025).
21. Wang, S. A. et al. Boric acid modified MOF-derived ni@c/al2O3-xB catalysts boosting the hydrodeoxygenation of guaiacol and raw bio-oil. *J. Anal. Appl. Pyrol.* **187**, 107025. https://doi.org/10.1016/j.jaap.
22. Zhang, R., Brown, R. C., Suby, A. & Cummer, K. Catalytic destruction of Tar in biomass derived producer gas. *Energ. Convers. Manage.* **45**, 995–1014 (2004).
23. Xu, X. M. *Study on Catalytic Hydrodeoxygenation Improvement of Biomass Pyrolysis Oil.* https://www.cnki.net) (Zhengzhou University, 2014).
24. Tan, Z. C. et al. Upgrading bio-oil model compounds phenol and furfural with in situ generated hydrogen. *Environ. Prog Sustain.* **33** (3), 751–755 (2014).
25. Jin, F. Q., Liu, P., Chen, L., Hua, D. L. & Yi, X. L. Study on the thermal stability of the bio-oil components by Py-GC/MS. *Energy Rep.* **9** (4), 280–288 (2023).
26. Hu, X. et al. Coke formation during thermal treatment of bio-oil. *Energ. Fuel* **34** (7), 7863–7914.
27. Alekseeva, M. V. et al. Effect of temperature on the hydrotreatment of sewage sludge-derived pyrolysis oil and behavior of Ni-based catalyst. *Catalysts* **10** (11), 1273 (2020).
28. Zhang, M. et al. A review of bio-oil upgrading by catalytic hydrotreatment: advances, challenges, and prospects. *Mol. Catal.* **504**, 111438. https://doi.org/10.1016/j.mcat.2021.111438 (2021).

29. Gil, A., Sancho-Sanz, I. & Korili, S. A. Progress and perspectives in the catalytic hydrotreatment of bio-oils: effect of the nature of the metal catalyst. *Ind. Eng. Chem. Res.* **63** (27), 11759–11775. https://doi.org/10.1021/acs.iecr.4c00747 (2024).
30. Lv, D. C. et al. Effective suppression of coke formation with lignin-derived oil during the upgrading of pyrolysis oils. *Biomass Bioenerg.* **159**, 106425. https://doi.org/10.1016/j.biombioe.2022.106425 (2022).
31. Rami, D. et al. Catalytic hydrotreating of Biooil and evaluation of main noxious emissions of gaseous phase. *Sci. Rep.* **11**, 6176. https://doi.org/10.1038/s41598-021-85244-z (2021).
32. Xu, X. et al. Upgrading of bio-oil using supercritical 1-butanol over ru/c heteroge Neous catalyst: role of solvent. *Energ. Fuel.* **28** (7), 4611–4621. https://doi.org/10.1021/ef500968a (2014).
33. Xu, X., Zhang, C., Zhai, Y., Liu, Y. & Zhang, R. Two-step catalytic hydrodeoxygenation of fast pyrolysis oil to hydrocarbon liquid fuels. *Chemosphere* **93**, 652–660 (2013).
34. Keramatian, Y., Li, C., Hu, X. & Gholizadeh, M. Co-pyrolysis of polyethylene terephthalate and Poplar wood: influence of zeolite catalyst on coke formation. *Biomass Convers. Biorefinery*. **13**, 16099–16113. https://doi.org/10.1007/s13399-022-02312-8 (2023).
35. Hoseini, M., Atashi, F., Gholizadeh, M. & Clarens, F. Coke formation and zeolite catalyst effects on products from co-pyrolysis of waste tyre and Poplar wood in a semi-batch reactor under N_2 atmosphere. *Energy Technol.* **12**, 1–17. https://doi.org/10.1002/ente.202300740 (2024).
36. Lemoupi-Ngomade, S. B. et al. Catalytic performances of CeO_2@SBA-15 as nanostructured material for biodiesel production from Podocarpus falcatus oil. *Chem. Eng. Res. Des.* **194**, 789–800. https://doi.org/10.1016/j.cherd.2023.05.010 (2023).
37. Lemoupi-Ngomade, S. B. et al. Pilot-scale optimization of enhanced biodiesel production from high FFA Podocarpus falcatus oil via simultaneous esterification and transesterification assisted by zirconia-supported ZSM-5. *Chem. Eng. Res. Des.* **209**, 52–66. https://doi.org/10.1016/j.cherd.2024.07.031 (2024).
38. Ulloa-Murillo, L. M. et al. Pyrolysis of municipal waste catalyzed with synthesized zeolite from steel making factory waste. *Sci. Rep.* **15**, 10556. https://doi.org/10.1038/s41598-025-95179-4 (2025).
39. Li, Y. et al. Coke deposition on Ni/HZSM-5 in bio-oil hydrodeoxygenation processing. *Energ. Fuel.* **29** (3), 1722–1728 (2015).
40. Li, Y. et al. Study of X-ray photoelectron spectroscopy on coke deposited on Ni/HZSM-5 in bio-oil hydrodeoxygenation. *React. Kinet Mech. Cat.* **117** (2), 801–813. https://doi.org/10.1007/s11144-016-0976-y (2016).
41. Yang, X. Q., Xu, S. P., Chen, Z. & Liu, J. T. Improved nickel-olivine catalysts with high coking resistance and regeneration ability for the steam reforming of benzene. *React. Kinet Mech. Cat.* **108** (2), 459–472. https://doi.org/10.1007/s11144-012-0527-0 (2013).
42. Li, Y. et al. Coke formation on the surface of Ni/HZSM-5 and Ni-Cu/HZSM-5 catalysts during bio-oil hydrodeoxygenation. *Fuel* **189**, 23–31. https://doi.org/10.1016/j.fuel.2016.10.047 (2017).
43. Alves, L. et al. Effect of macro-structure of Ni-based catalysts on methane splitting systems. *Fuel* **379**, 133115. https://doi.org/10.1016/j.fuel.2024.133115 (2025).
44. Nagappan, S. et al. Catalytic hydrothermal liquefaction of biomass into bio-oils and other value-added products -A review. *Fuel* **285**, 119053. https://doi.org/10.1016/j.fuel.2020.119053 (2021).
45. Bao, R. et al. A review of hydrothermal biomass liquefaction: operating parameters, reaction mechanism, and bio-oil yields and compositions. *Energ. Fuel.* **38** (10), 8437–8459. https://doi.org/10.1021/acs.energyfuels.4c00240 (2024).

Acknowledgements

This research was funded by the National Natural Science Foundation of China (21603061), the Natural Science Foundation of Henan Province (182300410168), Henan Province science and technology research project (242102310553) and the Key Scientific Research Projects of Colleges and University in Henan Province (23B150001).

Author contributions

X.X.: Conceptualization; methodology; formal analysis; investigation; data curation; writing-original draft preparation; resources; project administration; Y.W. and S.C.: formal analysis; investigation; data curation; P.L.: validation; supervision; W.G.: validation; resources; writing-review and editing; Y.S.: writing-review and editing. All authors have read and agreed to the published version of the manuscript.

Declarations

Competing interests

The authors declare no competing interests.

Additional information

Supplementary Information The online version contains supplementary material available at https://doi.org/10.1038/s41598-025-14087-9.

Correspondence and requests for materials should be addressed to X.X. or Y.S.